

---

---

## RESULTS OF JOINT OBSERVATIONS WITH SOLAR SPECTROPOLARIMETER OF METER RANGE WAVELENGTHS AND OTHER INSTRUMENTS

**N.O. Muratova**   
*Institute of Solar-Terrestrial Physics SB RAS,  
Irkutsk, Russia, muratova@iszf.irk.ru*

**A.Yu. Fedotova**   
*Institute of Solar-Terrestrial Physics SB RAS,  
Irkutsk, Russia, fedotovanastya@iszf.irk.ru*

**J.N. Shamsutdinova**   
*Institute of Solar-Terrestrial Physics SB RAS,  
Irkutsk, Russia, yulia@iszf.irk.ru*

---

**Abstract.** Solar radiation is emitted in the wide frequency range from gamma to radio emission. Hence, joint observations from different instruments and frequency ranges let us to complete full representation of the evolution of solar events and confirm authenticity of data from specific instruments. In this article, we present comparative analysis data from Solar Spectropolarimeter of Meter Range wavelengths (SSMD) and other instruments. For the investigation we have chosen three solar events registered with SSMD in 2019: type III radio bursts on May 6 from 05:05 UT to 05:12 UT, type II radio bursts on May 6 from 05:12 UT to 05:19 UT, and type III radio bursts on April 14 from 05:03 UT to 05:21 UT. For comparison we apply data from the following instruments: SSMD, SRH (Siberian Radioheliograph), SDO/AIA (Atmospheric Imaging Assembly (AIA) on the Solar Dynamics Observatory (SDO)),

Wind/WAVES (WAVES investigation on the WIND spacecraft), ground-based spectropolarimeter AMATERAS, spacecraft GOES-14. As a result, we can conclude that they are in good correlation with each other and correspond to outstanding characteristics for each event. The investigation also confirms the SSMD data authenticity.

**Keywords:** Sun, radio radiation, type II radio bursts, type III radio bursts, solar flares, solar events, instruments.

---

## INTRODUCTION

Solar radiation is detected in a wide frequency range — from gamma to radio emission. Comparison of data from different instruments in several frequency ranges when studying solar activity allows us to analyze selected phenomena, to recreate a complete picture of the development of solar events, and to verify the truth of the occurrence of these events. For this purpose, we use data from both space and ground-based instruments.

The aim of this work is to examine the events recorded by the Solar Spectropolarimeter of meter range wavelengths (SSMD) [Muratova et al., 2019] together with other instruments in different frequency ranges and to confirm their reliability.

In the meter waveband, a huge number of solar phenomena appearing as radio bursts of various types can occur. Their first observations began in 1942 with the discovery of solar radio emission. Many papers were devoted to such observations (for example, [Appleton et al., 1946; McCready et al., 1947; Payne-Scott, 1949]). One of the first classifications of radio bursts was presented by Wild [Wild et al., 1963]. In this paper, we deal with events associated with type II and III radio bursts [Wild, McCready, 1950]. Type III includes radio bursts with a fast frequency drift, which are produced by nonthermal electrons propagating along open field lines from the Sun into the interplanetary medium. Type II

includes radio bursts with a slow frequency drift. Electrons accelerated by shock waves propagating in the solar corona are involved in their formation. We have used data acquired with SSMD. We have selected three events occurring in 2019 for the study: radio bursts of types III (at 05:05–05:11 UT) and II (at 05:12–05:19 UT) recorded on May 6, and a group of type III radio bursts (at 05:04–05:20 UT) detected on April 14.

To confirm the events under study, we present data from AMATERAS in the 100–500 MHz frequency range. The fact that the events propagate to higher layers of the solar atmosphere is evident from the data obtained with the Wind/WAVES instruments — RAD1 (20–1040 kHz) and RAD2 (1.075–13.825 MHz). We present the data from these instruments from 05:00 to 05:30 UT for the events of May 6 and from 05:00 to 05:40 UT for the events of April 14 as combined spectra.

In lower layers of the solar atmosphere, we can observe the "prehistory" of the phenomena considered. For this purpose, we have used data from the Siberian Radioheliograph (SRH) [Altyntsev et al., 2020] and SDO/AIA [Lemen et al., 2012]. The first event associated with an M1.0-class flare was examined from 05:00 to 05:08 UT; and the second during a C9.9 class flare, from 05:10 to 05:17 UT on May 6. The third event related to an A8.0-class flare was analyzed from 05:10 to 05:17 UT and from 05:14 to 05:30 UT on April 14.

For each event, we present X-ray fluxes derived

from GOES-14 data, as well as microwave emission fluxes from SRH data at a frequency of 5.125 GHz.

The next section takes a closer look at the observation instruments and methods involved in data analysis.

## INSTRUMENTS AND OBSERVATION METHODS

The Solar Spectropolarimeter of meter range wavelengths is a radio spectropolarimeter designed to observe solar radio bursts of various types in the 50–500 MHz range. SSMD successfully began regular observations at the ISTP SB RAS Radio Astrophysical Observatory (the Badary area) in April 2016. The observations were made from 2016 to 2020. A log-periodic crossed antenna is installed at the input of the receiver that simultaneously receives horizontal and vertical polarization components. The main parameters of SSMD are: 4608 frequency channels, the channel width and the step between them are 97.656 kHz, the time resolution is 1 s. We use the intensity (Stokes  $I$ ). The instrument is described in detail in [Muratova et al., 2019]. Note that observations in this range are complicated by the presence of various interference effects both of artificial origin (from other radio electronic devices) and from some natural phenomena [<https://www.slideserve.com/toussaint/srs-data-examples-powerpoint-ppt-presentation>]. The SSMD data catalog for the period 2016–2020 is currently under development. The data can be obtained upon request from N.O. Muratova.

To clean images, in each frequency channel we found the median value of the initial signal intensity for a certain time interval, which was then subtracted from it; upon which we divided the resulting values by the standard deviation in the channel. Due to the presence of interference of different types, the entire 50–500 MHz range was conditionally subdivided into three parts, each processed and displayed separately. The data is not calibrated and is presented in relative units.

The Siberian Radioheliograph (SRH) is a multiwave T-shaped radio interferometer designed to record phenomena on the Sun in the 3–24 GHz frequency range [<http://ckp-rf.ru/usu/73606>]. The instrument is developed in the Badary area. Until 2020, an SRH prototype operated in the 4–8 GHz frequency band with a spatial resolution of 21'. Since 2021, the radio interferometer has been working in the test mode in the 3–6 GHz band. The instrument is currently under construction and it is planned to put the arrays into operation in the 6–12 GHz band and then in the 12–24 GHz band [Altyntsev et al., 2020]. The SRH data provided profiles of microwave emission fluxes, as well as spatial images of radio brightness of the solar disk at several frequencies.

GOES-14 (GOES-O) is an environmental satellite [[https://www.noaa.gov/GOES/GOES\\_DCS/goes\\_dcs.html](https://www.noaa.gov/GOES/GOES_DCS/goes_dcs.html)], but its observations are also useful in monitoring solar activity. The GOES-14 data was used to construct X-ray flux profiles for flares in the 1–8 Å range. The data is available at [<https://hesperia.gsfc.nasa.gov/goes/>].

To visualize the evolution of the events and to construct brightness temperature profiles, we have used full-disk solar images in the SDO/AIA EUV171, 304,

and 94 Å channels with a cadence of 12 s and a spatial resolution of 0.6" [Lemen et al., 2012]. The SDO data is available at [<https://sdo.gsfc.nasa.gov/data/aiahmi>].

AMATERAS is a broadband meter radio spectropolarimeter designed to observe solar radio bursts in a 150–500 MHz frequency range (note that according to the data for 2019 the range was 100–500 MHz). The number of channels is 16384; the time resolution is 10 ms. The instrument records right-hand and left-hand circular polarizations [Iwai et al., 2012].

WAVES is an instrument installed in the WIND spacecraft. It detects plasma and radio waves of solar origin, using RAD1, RAD2 receivers. The RAD1 frequency range is 20–1040 kHz, the number of channels is 256, and the time resolution is 1 min. The RAD2 frequency range is 1.075–13.825 MHz, the number of channels is 256, and the time resolution is 1 min [Bougret et al., 1995].

We present the AMATERAS, Wind/WAVES data for each event in the form of combined spectra. To analyze the events under study, we have developed software capable of simplifying and automating the visualization of dynamic spectra in the meter range. The software automatically downloads data from the instruments' servers by event date in FITS or SAV format, then reads and processes the files.

The data processing algorithm works with data arrays and takes all characteristics of each instrument into account for further selection of the area of interest for a given period of time. Then, the data array is processed to improve the image quality. To do this, a histogram equalization method is used to increase the contrast of low-contrast areas. Histogram equalization is performed by distributing the most frequent intensity values, thereby making it possible to isolate flares from the general background.

As a result, the software performs the following tasks: reading files, calibrating (transferring data from dB·m to sfu), preprocessing, arranging data from different instruments, taking into account their frequency range and intensity values. At the end of this process, we get images of dynamic radio spectra in the meter range at a given time interval.

## OBSERVATIONS AND DATA ANALYSIS

The first two events we discuss occurred on May 6, 2019. Figure 1 shows a dynamic intensity spectrum (Stokes  $I$ ) constructed for the group of type III radio bursts recorded by SSMD on May 6, 2019 at 05:05–05:12 UT. The event lasted for several minutes. This image displays the fine structure in the form of single short radio bursts with a duration of 1 s (SSMD resolution is 1 s) with a fast frequency drift from high to low frequencies at a velocity of  $-13$  to  $-20.67$  MHz·s $^{-1}$  as the event propagates in upper layers of the solar atmosphere. In some places, we can see pronounced continuous emission whose intensity also changes during the event evolution. This event covers a wide frequency range from 50 MHz (the lower limit of the SSMD frequency range) to 360 MHz. All of the above features are characteristic for type III radio bursts [[https://www.sws.bom.gov.au/World\\_Data\\_Centre/1/9/5](https://www.sws.bom.gov.au/World_Data_Centre/1/9/5)].

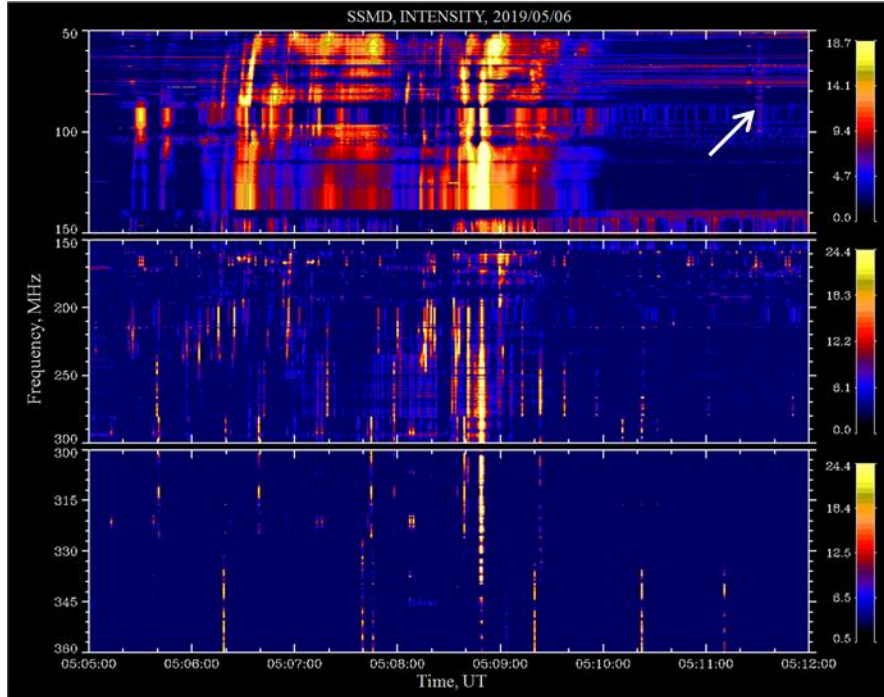


Figure 1. Dynamic intensity spectrum of a group of type III radio bursts obtained from SSMD data for 05:05–05:12 UT on May 6, 2019. The white arrow indicates a weak type III radio burst.

Spectral images are not uniform in frequency; for example, the presence of interference in the 140–160 MHz range, which was mentioned above, did not provide a higher quality image. The event began at 05:05 UT with single radio bursts, occupying an ever wider frequency range as it developed. The peak of the event, according to the obtained spectrum, was recorded at 05:08 UT, and by 05:10 UT it fades away. We also see a weak type III radio burst at 05:11:30 UT in the 50–110 MHz frequency range (white arrow in Figures 1 and 6).

On the combined spectrum shown in Figure 2 according to AMATERAS data, a group of type III radio bursts is visible in the 100–500 MHz frequency range from 05:05 to 05:10 UT with a fast frequency drift. The maximum is at 05:08 UT. In the upper layers of the solar atmosphere, according to the data from Wind/WAVES RAD1 (05:07–05:16 UT) and RAD2 (05:09–05:30 UT and beyond), a continuous high-intensity type III radio burst is observed.

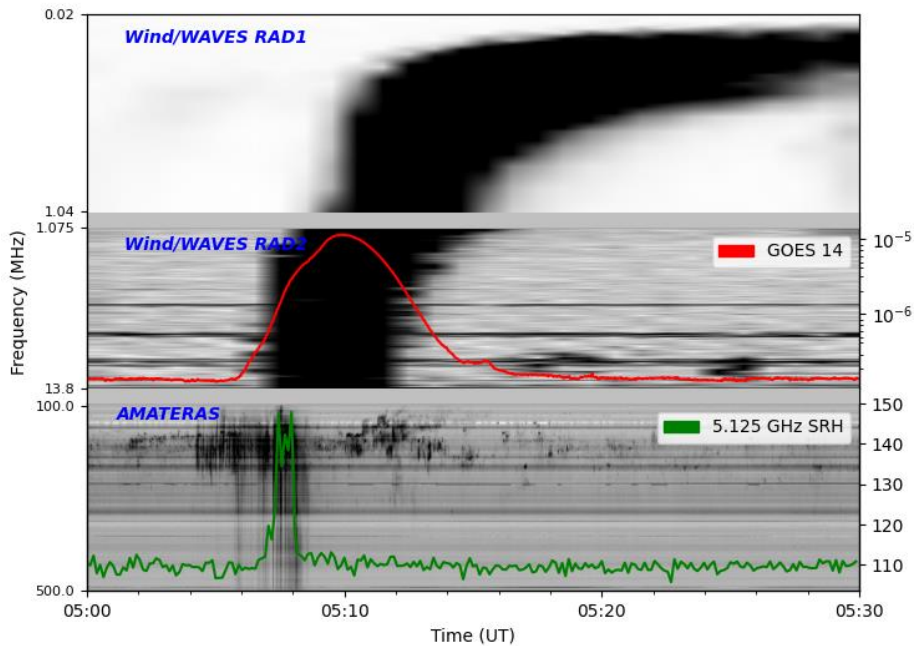


Figure 2. Combined spectrum for two events on May 6, 2019, which shows dynamic spectra derived from AMATERAS and Wind/WAVES data, as well as the microwave emission flux recorded by SRH at a frequency of 5.125 GHz, and the X-ray flux profile from GOES-14 in the 1–8 Å range

According to the profile of the total microwave emission flux presented in Figure 2 from SRH data at a frequency of 5.125 GHz, from 05:07 to 05:12 UT there are three peaks with maxima from 142 to 149 sfu. As inferred from GOES-14 data, the X-ray emission at the flare maximum is  $10^{-6} \text{ W}\cdot\text{m}^{-2}$ .

We also analyze this event, using SRH and SDO/AIA spatial images. At 05:05–05:08 UT, an M1.0-class flare occurred on the solar disk near the active region (AR) NOAA 12740 [[https://suntoday.lmsal.com/suntoday/?suntoday\\_date=2019-05-06](https://suntoday.lmsal.com/suntoday/?suntoday_date=2019-05-06)].

Figure 3 presents a full disk solar image for 05:08 UT on May 6, 2019 according to SDO/AIA data at a wavelength of 94 Å. In the northwestern part of the disk, the white rectangle (270"×246") marks the flare at its maximum phase.

Figure 4, *a–c* displays SDO/AIA spatial images of the flare at the 94, 304, and 131 Å wavelengths, which trace the emission increase; and the maximum phase of the flare is at 05:08 UT. Contours indicate the microwave emission of the flare according to SRH data at a frequency of 6.0 GHz at 0.5, 0.7, and 0.9 levels of maxima of brightness temperature maps.

The second event of interest is a type II radio burst with a slow drift from high to low frequencies (Figure 5). The drift velocity is  $-0.308 \text{ MHz}\cdot\text{s}^{-1}$ . This event occurred almost immediately after the type III burst (see Figure 1) within 2 min of one another (excluding the single weak burst at 05:11:30 UT), which is a typical situation [[https://www.sws.bom.gov.au/World\\_Data\\_Centre/1/9/5](https://www.sws.bom.gov.au/World_Data_Centre/1/9/5)].

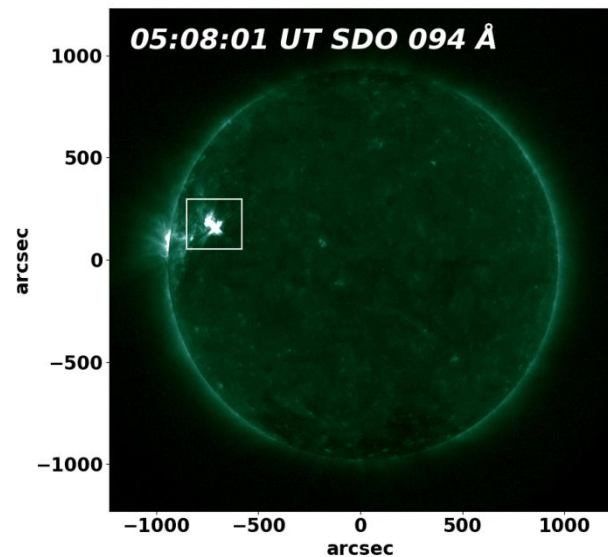


Figure 3. Full disk solar image from SDO/AIA data at a wavelength of 94 Å for May 6, 2019. The white rectangle 270"×246" marks the region of the maximum stage of the M1.0-class flare at 05:08 UT

At 05:11:30 UT, we see a short weak type III burst, then at ~05:12 UT a type II burst begins, which lasts for several minutes, to ~05:19 UT. The type II burst occupies mainly the lower part of the spectrum from 75–150 MHz; its fragments are also present at higher frequencies from 150 to 230 MHz and at lower frequencies 50–

75 MHz. In the 150–180 MHz range, strong interference was observed which prevented the signal from being isolated in this range. The event considered was more intense than the previous one.

Having analyzed the combined spectra in Figure 2 from AMATERAS data, we also see a type II radio burst in the 100–200 MHz frequency range at 05:11–05:20 UT. In the upper part of the RAD2 range (from ~10 kHz and above) from 05:15 to 05:26 UT, the event is faint. We did not manage to detect a response to the flare from the profile of the total microwave emission flux. The X-ray emission profile according to GOES-14 data has the form of a gentle slope. The maximum X-ray emission is observed at 05:15 UT and is  $10^{-6} \text{ W}\cdot\text{m}^{-2}$ .

In the northwestern part of the solar disk near AR NOAA 12740, spatial images show a flare from 05:10 to 05:17 UT, which corresponds to class C9.9 according to [[https://suntoday.lmsal.com/suntoday/?suntoday\\_date=2019-05-06](https://suntoday.lmsal.com/suntoday/?suntoday_date=2019-05-06)]. Evolution of the flare from 05:10 to 05:15 UT according to SDO/AIA data is illustrated in Figure 6 at wavelengths of 94 (*a*), 304 (*b*), and 131 Å (*c*). All the wavelengths exhibit a gradual decrease in brightness, and the flare peaked at 05:10 UT. Contours indicate the microwave emission of the flare according to SRH data at a frequency of 6.0 GHz at 0.5, 0.7, and 0.9 levels of maxima of brightness temperature maps.

According to [[https://aia.lmsal.com/aia\\_cadence/aia\\_0193\\_rdiff\\_0144\\_sum\\_20190506\\_0500/AIA\\_0193\\_RDIF0144\\_SUM\\_20190506\\_0500.html](https://aia.lmsal.com/aia_cadence/aia_0193_rdiff_0144_sum_20190506_0500/AIA_0193_RDIF0144_SUM_20190506_0500.html)] on the website [[https://suntoday.lmsal.com/suntoday/?suntoday\\_date=2019-05-06](https://suntoday.lmsal.com/suntoday/?suntoday_date=2019-05-06)], at 05:01:28–05:39:28 UT in the same AR a coronal shock wave occurred which, according to our assumptions, is related to the type II coronal radio burst [Cairns et al., 2000] detected by SSMD and AMATERAS in the 50–250 MHz range (see Figures 2, 5).

The last event we analyze (Figures 7, 8) consists of type III radio bursts recorded on April 14, 2019.

On the whole, the event has the character of a noise storm and appears on the spectra as groups and individual type III radio bursts that follow intermittently throughout the observation day. The event is long, so we have presented only two fragments of the dynamic spectra — from 05:03 to 05:09 UT and from 05:14 to 05:21 UT. The former fragment (Figure 7) is a group of weak type III radio bursts with continuous background emission, in which we can isolate a weak fine structure and an intense burst at 05:05 UT. The latter fragment (Figure 8) shows a group of more intense radio bursts (beginning at ~05:15 UT) with a higher level of continuous emission than in the former fragment. Radio bursts at 05:16 UT and three intense radio bursts at the end of the group in the period from 05:18 to 05:19 UT are clearly defined. By 05:20 UT, the event fades. The drift velocity of individual radio bursts for the two fragments varies from  $-13.2$  to  $-26.67 \text{ MHz}\cdot\text{s}^{-1}$ . The event occupies predominantly the lower part of the SSMD spectrum, from 50 to 160 MHz, and continues for a long time, manifested in groups and individual bursts.

The combined spectrum (Figure 9) from 05:00 to 05:21 UT, according to AMATERAS data, in the range of 100–200 MHz exhibits many barely noticeable type III radio bursts.

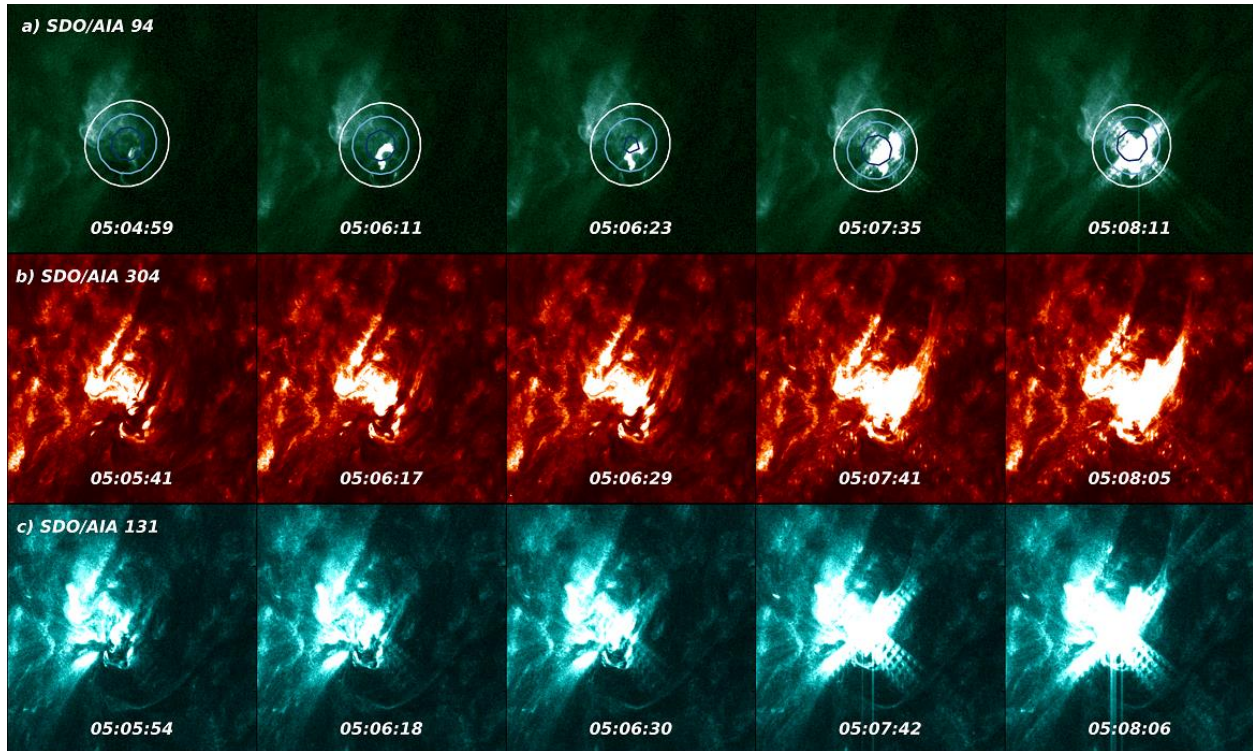


Figure 4. Spatial images of the May 6, 2019 flare from 05:05 to 05:08 UT according to SDO/AIA data at wavelengths of 94, 304, and 131 Å (a–c). Contours depict microwave emission derived from SRH data at a frequency of 6.0 GHz at levels of 0.5 (blue line), 0.7 (light blue line), and 0.9 (white line) of brightness temperature maxima. Frame size is  $125'' \times 125''$

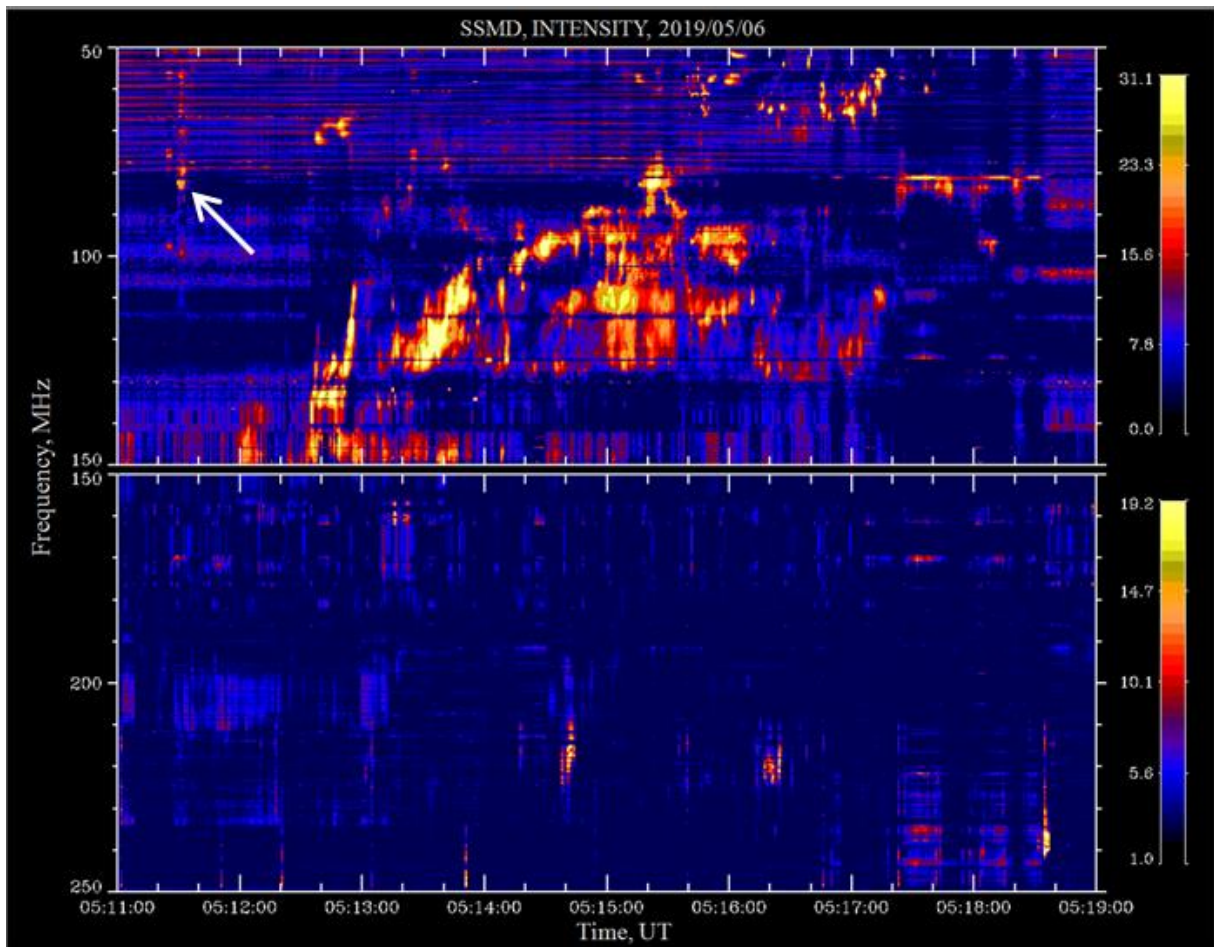


Figure 5. Dynamic intensity spectrum of a type II radio burst, constructed from SSMD data for 05:11–05:19 UT on May 6, 2019

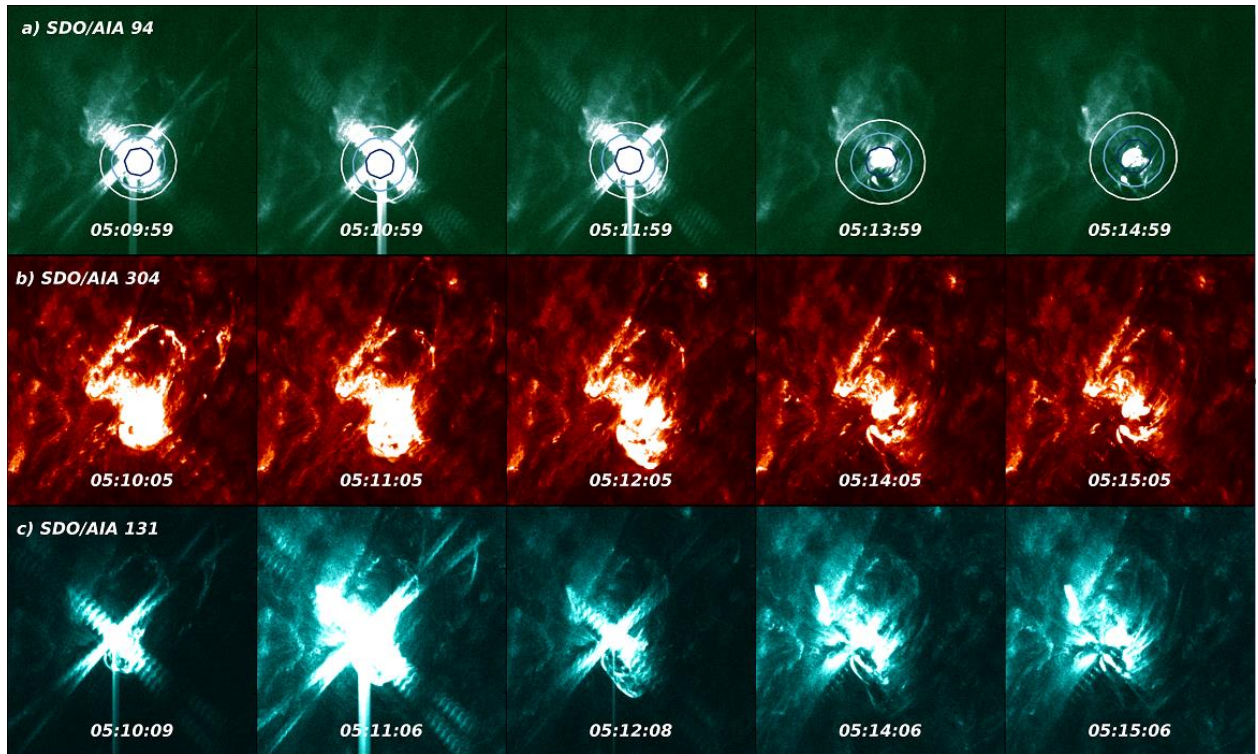


Figure 6. Spatial images of the May 6, 2019 flare from 05:10 to 05:15 UT, obtained from SDO/AIA data at wavelengths of 94, 304, and 131 Å (a–c). Contours depict microwave emission derived from SRH data at a frequency of 6.0 GHz at levels of 0.5 (blue line), 0.7 (light blue line), and 0.9 (white line) of brightness temperature maxima. Frame size is 125"×125"

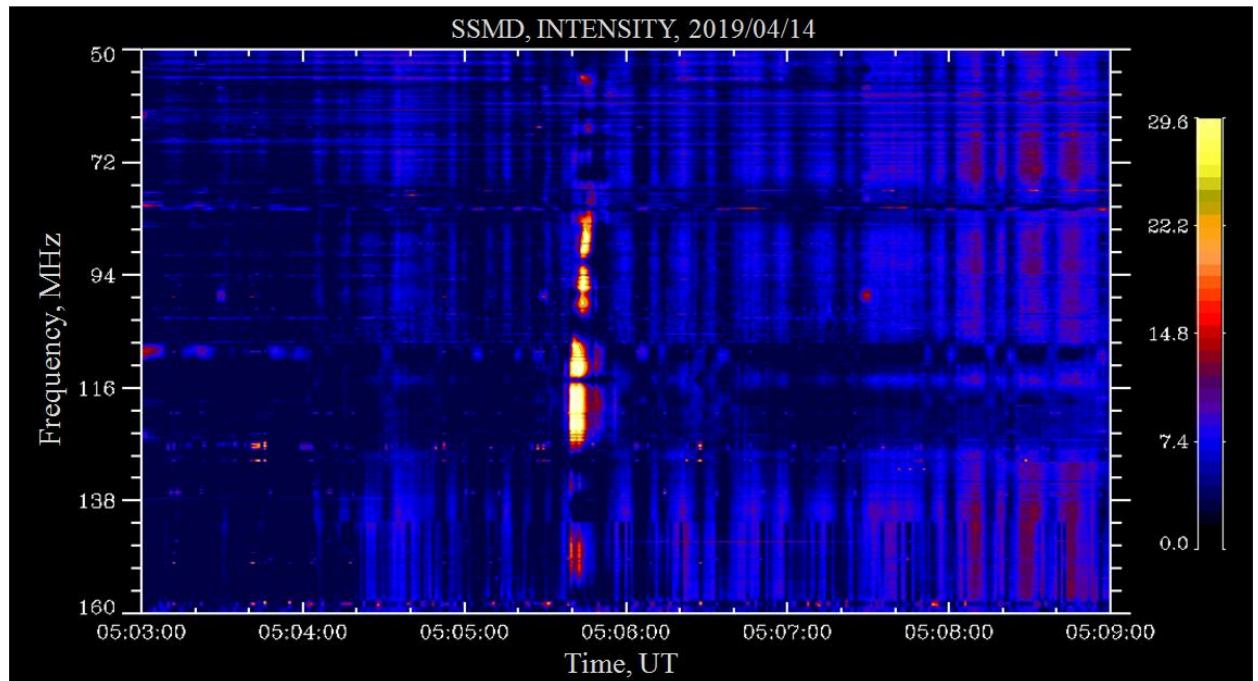


Figure 7. Dynamic intensity spectrum of a group of type III radio bursts, recorded by SSMD on April 14, 2019, for 05:03–05:09 UT

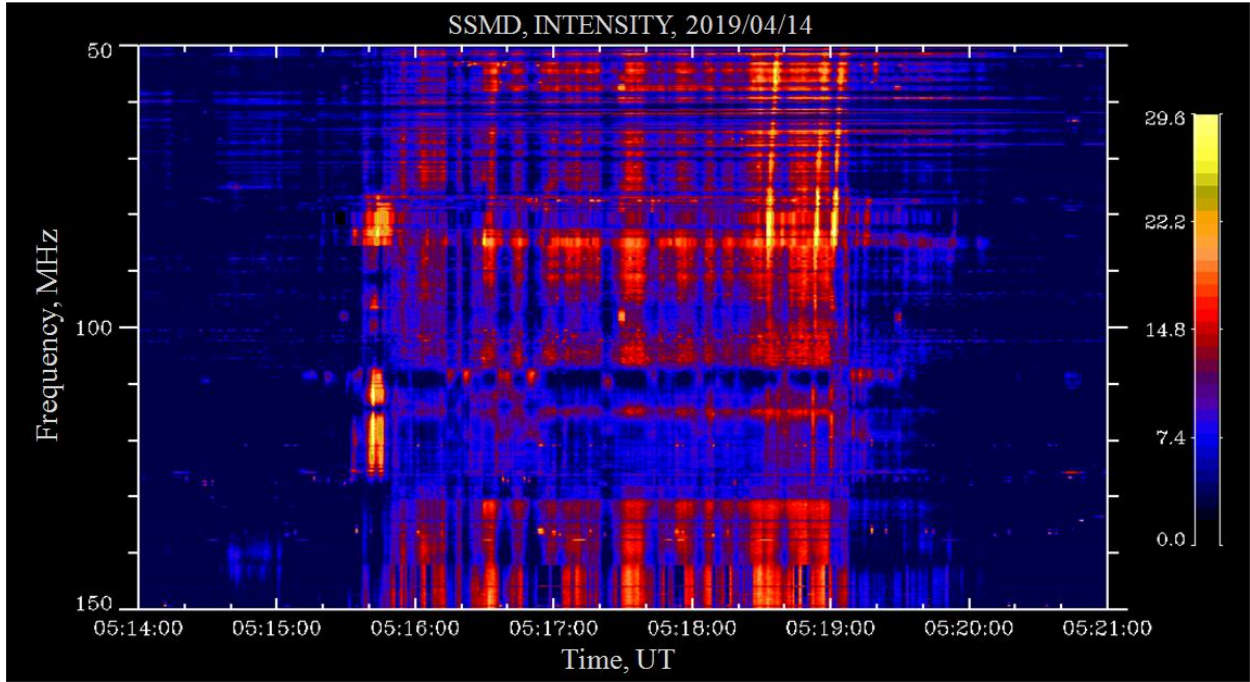


Figure 8. Dynamic intensity spectrum of a group of type III radio bursts, recorded by SSMD on April 14, 2019, for 05:14–05:21 UT

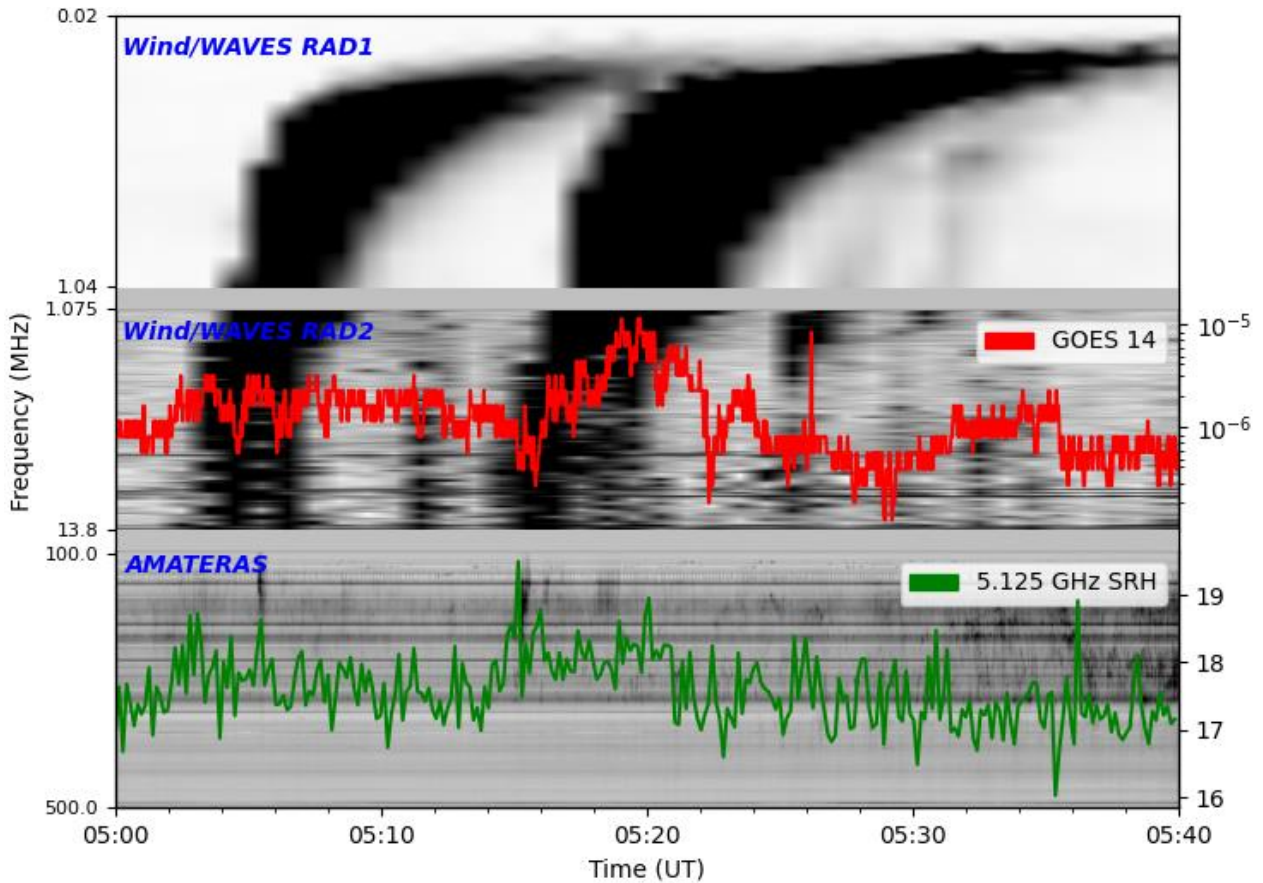


Figure 9. Combined spectrum for the April 14, 2019 events, which exhibits dynamic spectra according to AMATERAS and Wind/WAVES data, as well as the total microwave emission flux from SRH data at a frequency of 5.125 GHz and the X-ray flux profile from GOES-14 at 1–8 Å

In general, the event is a noise storm in nature. Radio bursts at 05:06 and 05:15 UT stand out well against the background of numerous bursts. Some small

bursts that are above 150 MHz in the range are likely to form type I noise storms. Such activity was observed by the radiospectrograph of the Learmonth

Observatory all through the day [[https://www.sws.bom.gov.au/World\\_Data\\_Centre/1/9/6](https://www.sws.bom.gov.au/World_Data_Centre/1/9/6)]. According to Wind/WAVES data, two high-intensity type III radio bursts can be distinguished in the upper layers (the first begins at 05:03 UT, the second at 05:14 UT), which are continuous.

According to SRH data (green curve), at a frequency of 5.125 GHz from 05:00 to 05:14 UT there is an inhomogeneous increase in the microwave emission flux with a 16–18 sfu intensity. From 05:15:00 to 05:23:00 UT, there are also several bursts of radio emission from 19.5 to 18.2 sfu.

From the GOES-14 X-ray emission profile (red curve) at 05:01–05:05 UT, it is impossible to isolate the flare due to intense background noise at the level of  $10^{-6}$  W·m<sup>-2</sup>. However, from 05:15 to 05:22 UT, the flare profile is clearly pronounced, the value at the maximum is  $10^{-6}$  W·m<sup>-2</sup>. The background emission flux until 05:40 UT changes slightly. Figure 10 shows the full solar disk according to SDO/AIA data at the wavelength of 94 Å at 05:18 UT. The white rectangle denotes the flare in the form of a complex system of loops with a bright narrow filament in its lower right part.

In spatial images (Figure 11), an A8.0-class flare of complex configuration was distinguished in AR N12W00. On panels are SDO/AIA images captured at wavelengths of 304 (a), 171 (b), 335 Å (b). For example, Figure 11, a shows a bright source at 05:00 UT, which fades a little at 05:02 UT, then flares up again and hardly changes further. Contours indicate the microwave emission of the flare as derived from SRH data at a frequency of 6.0 GHz at levels of 0.5, 0.7, and 0.9 of brightness temperature maxima.

From 05:13 to 05:19 UT, the flare was observed, according to SDO/AIA data, at wavelengths of 304, 171, and 335 Å (Figure 12). Figure 12 traces the evolution of the flare (as a bright filament). Contours indicate the microwave emission of the flare as derived from SRH data at a frequency of 6.0 GHz at levels of 0.5, 0.7, and 0.9 of brightness temperature maxima.

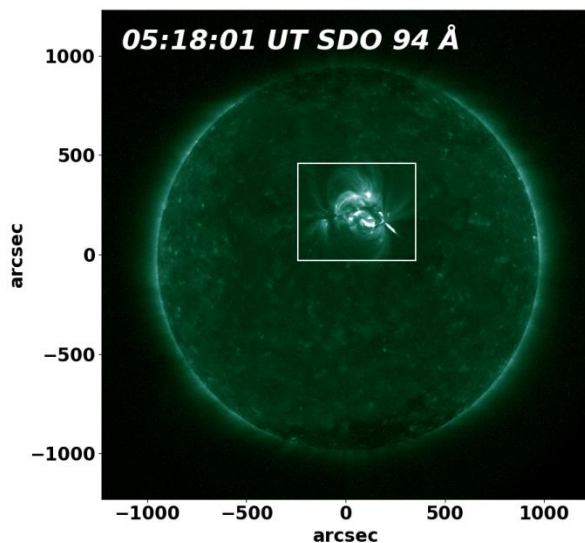


Figure 10. Full disk solar image from SDO/AIA data for 05:18 UT on April 14, 2019 at a wavelength of 94 Å. The white rectangle marks an A8.0 flare region of 492"×600"

## CONCLUSION AND DISCUSSION

We have used data from several instruments to analyze three events in 2019 recorded with SSMD: the first event – on May 6 from 05:05 to 05:12 UT, the second – from 05:12 to 05:19 UT, and the third – on April 14 from 05:03 to 05:09 UT and from 05:14 to 05:21 UT.

The group of type III radio bursts occupying a wide frequency range was considered as the first event. The bursts feature a fast frequency drift (the drift velocity of individual bursts ranged from  $-13$  to  $-20.67$  MHz·s<sup>-1</sup>). There is also a fine structure (see Figure 1) in the form of single short radio bursts with duration of 1 s and pronounced continuous emission. Comparative analysis has shown the following: a group of type III bursts according to AMATERAS data and an intense type III burst according to Wind/WAVES RAD1 and RAD2 data; responses with maxima from 142 to 149 sfu in the microwave emission flux, which occurred in NOAA 12740 AR (as derived from SDO/AIA data at a wavelength of 94 Å, see Figure 3); one wide response to the M1.0-class flare in the X-ray flux profile from GOES-14.

A type II radio burst was considered as the second event (see Figure 5). This event follows almost immediately after the type III radio burst and features a slow frequency drift ( $-0.308$  MHz·s<sup>-1</sup>). Comparison between data from different instruments shows a type II radio burst according to AMATERAS data and a weak manifestation of the event according to Wind/WAVES RAD2 data; RAD1 did not detect any activity. The GOES-14 X-ray flux profile reveals a weak response to the C9.9-class flare. Spatial images according to SDO/AIA data at wavelengths of 94, 304, and 131 Å exhibit a decaying flare with maximum at 5:10 UT. In the same period, SDO/AIA difference images at wavelengths of 335, 211, and 193 Å display a shock wave in the same AR NOAA 12740. We assume that the coronal shock wave might have led to the formation of the type II coronal radio burst detected by SSMD and AMATERAS.

As the third event (see Figures 7, 8) we considered two groups of type III radio bursts (in general, the event lasted throughout April 14 as groups and individual radio bursts). This is an event with a narrower spectrum compared to the first event considered (see Figure 1). The drift velocity of individual bursts ranged from  $-13.2$  to  $-26.67$  MHz·s<sup>-1</sup>. Against the background of the bursts there is continuous emission, which is more intense from 05:14 to 05:21 UT. At the beginning of each group, individual type III bursts are well distinguished; at the end of the second group, several short-lived narrow-band bursts are visible. In this case, comparison with other instruments has revealed the following: AMATERAS data shows many barely noticeable type III radio bursts forming a noise storm, against which a pair of more intense radio bursts stand out sharply; from Wind/WAVES data, two intense type III radio bursts are well traced; according to SRH data at a frequency of 5.125 GHz the microwave emission profile exhibits an increase in the flux and two responses to the flare. Due to the high noise level, it is impossible to distinguish the flare from the GOES-14

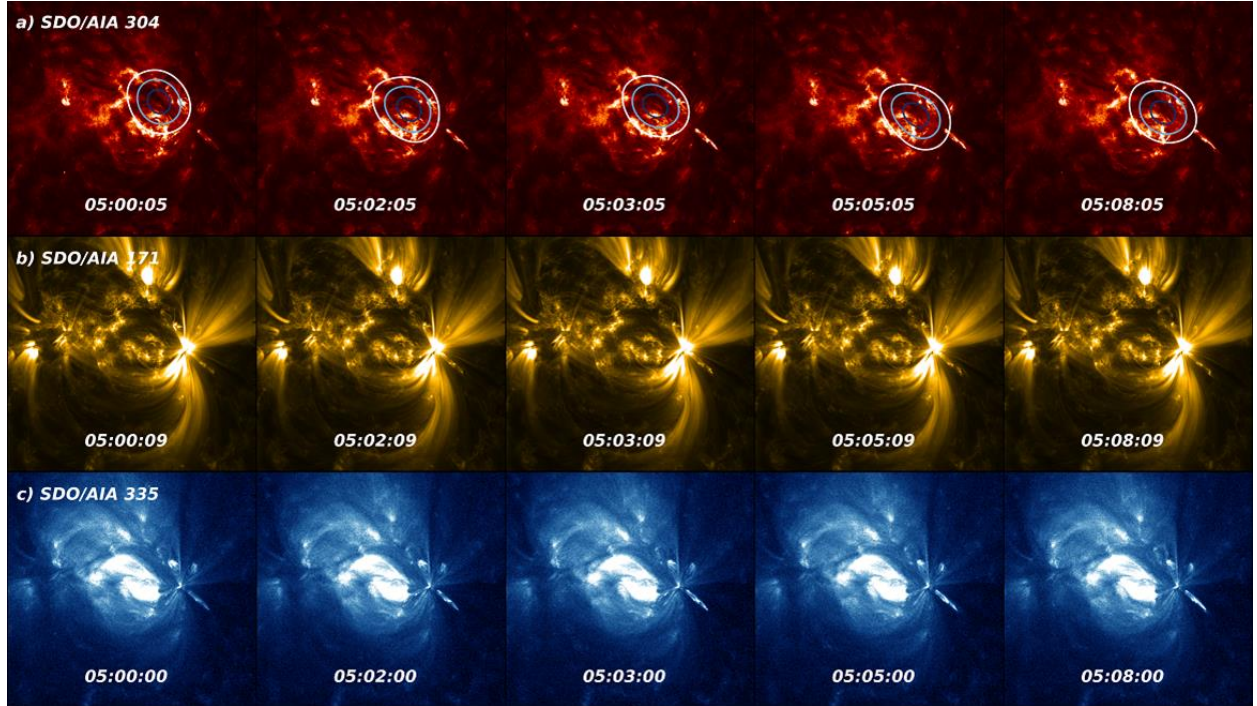


Figure 11. Evolution of the A8.0-class flare in spatial images according to SDO/AIA data at wavelengths of 304, 171, and 335 Å (a–c) from 05:00 to 05:08 UT on April 14, 2019. Frame size is  $400'' \times 400''$ . Contours indicate the microwave emission of the flare derived from SRH data at a frequency of 6.0 GHz at levels of 0.5 (blue line), 0.7 (light blue line), and 0.9 (white line) of brightness temperature maxima

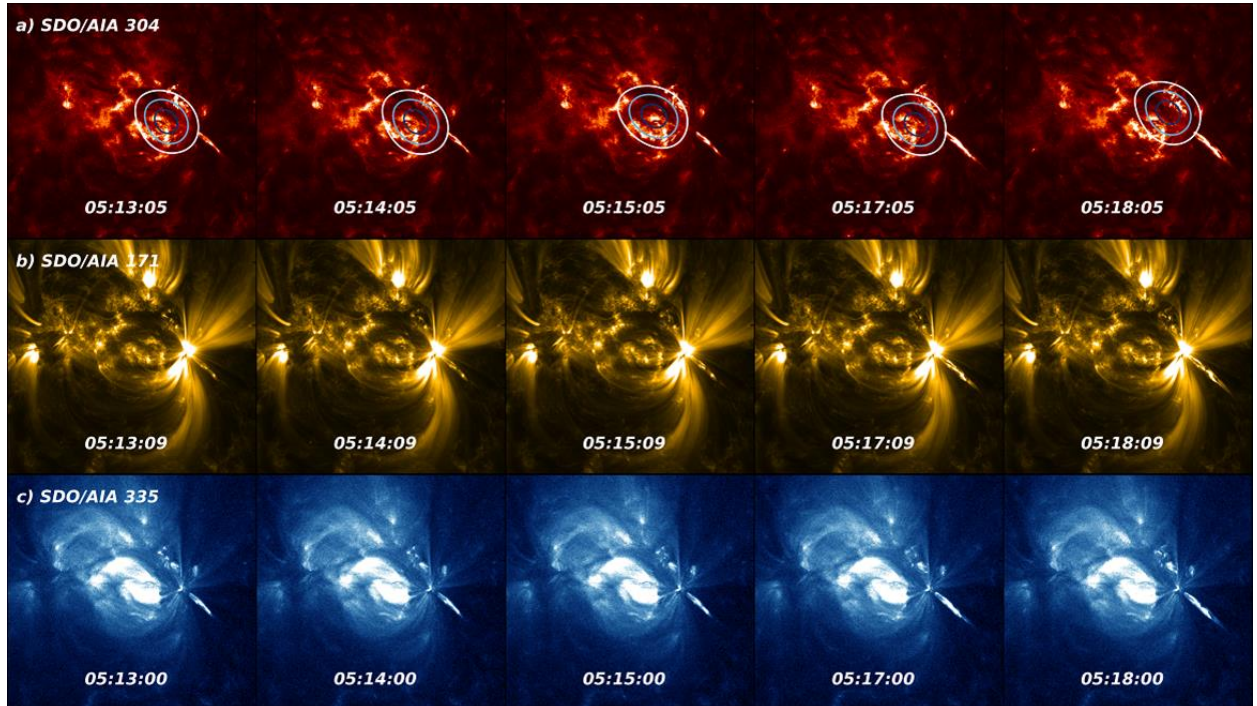


Figure 12. Evolution of the A8.0-class flare in spatial images according to SDO/AIA data at wavelengths of 304, 171, and 335 Å (a–c) from 05:14 to 05:18 UT on April 14, 2019. Frame size is  $400'' \times 400''$ . Contours indicate the microwave emission of the flare according to SRH data at a frequency of 6.0 GHz at levels of 0.5 (blue line), 0.7 (light blue line), and 0.9 (white line) of the maximum brightness temperature

X-ray emission profile. In AR N12W00, the A8.0-class flare shown in the SDO/AIA image at a wavelength of 94 Å was observed. Spatial images from SDO/AIA at 304 and 171 Å show a flare of a complex configuration; and a region in the form of an upward

bright narrow filament is well defined. However, according to SRH data, at frequencies of 4.5 and 5.125 GHz the flare changed little.

The results of analysis of data from different instruments show that they correlate well with each other and

correspond to characteristic features of each event. Thus, due to the joint observations we have obtained a complete picture of the development of the events recorded with SSMD and confirmed their validity.

We thank reviewers for editing the article. We are grateful to WAVES, SWAVES, GOES, SDO/AIA teams for providing open access to their observational data. The results were obtained using the Solar Spectropolarimeter of meter range wavelengths (SSMD) and the Unique Research Facility "Siberian Solar Radio Telescope" [<http://ckp-rf.ru/usu/73606>].

The work was financially supported by the Ministry of Science and Higher Education of the Russian Federation (N.O. Muratova, A.Yu. Fedotova, Yu.N. Shamsutdinova), RFBR, and the Royal Society of London (Grant No. 21-52-10012 KO\_a, Yu.N. Shamsutdinova).

## REFERENCES

- Altynsev A., Lesovoi S., Globa M., Gubin A., Kochanov A., Grechnev V., et al. Multiwave Siberian Radioheliograph. *Solar-Terr. Phys.* 2020, vol. 6, iss. 2, pp. 30–40. DOI: [10.12737/stp-62202003](https://doi.org/10.12737/stp-62202003).
- Appleton E.V., Hey J.S. Circular polarization of solar radio noise. *Nature*. 1946, vol. 158, iss. 4010, p. 339. DOI: [10.1038/158339a0](https://doi.org/10.1038/158339a0).
- Bougeret J.-L., Kaiser M.L., Kellogg P.J., Manning R., Goetz K., Monson S.J., et al. WAVES: The radio and plasma wave investigation on the Wind spacecraft. *Space Sci. Rev.* 1995, vol. 71, iss. 1-4, pp. 231–263. DOI: [10.1007/BF00751331](https://doi.org/10.1007/BF00751331).
- Cairns I.H., Robinson P.A., Zank G.P. Progress on coronal, interplanetary, foreshock, and outer heliospheric radio emissions. *Publ. Astron. Soc. Aust.* 2000, vol. 17, iss. 1, pp. 22–34. DOI: [10.1071/AS00022](https://doi.org/10.1071/AS00022).
- Iwai K., Tsuchiya F., Morioka A., Misawa H. IPRT/AMATERAS: A new metric spectrum observation system for solar radio bursts. *Solar Phys.* 2012. Vol. 277, iss. 2. P. 447–457. DOI: [10.1007/s11207-011-9919-y](https://doi.org/10.1007/s11207-011-9919-y).
- Lemen J.R., Title A.M., Akin D.J., et al. The Atmospheric Imaging Assembly (AIA) on the Solar Dynamics Observatory (SDO). *Solar Phys.* 2012, vol. 275, iss. 1-2, pp. 17–40. DOI: [10.1007/s11207-011-9776-8](https://doi.org/10.1007/s11207-011-9776-8).
- McCready L.L., Pawsey J.L., Payne-Scott R. Solar radiation at radio frequencies and its relation to sunspots. *Proc. Roy. Soc. A: Math. and Phys. Sci.* 1947, vol. 190, iss. 1022, pp. 357–375. DOI: [10.1098/rspa.1947.0081](https://doi.org/10.1098/rspa.1947.0081).
- Muratova N., Muratov A., Kashapova L. Results of work of new spectropolarimeter for solar radio emission observations in the range 50–500 MHz. *Solar-Terr. Phys.* 2019, vol. 5, iss. 3, pp. 3–9. DOI: [10.12737/stp-53201901](https://doi.org/10.12737/stp-53201901).
- Payne-Scott R. Bursts of solar radiation at metre wavelengths. *Austral. J. Sci. Res. A.* 1949, vol. 2, pp. 214–227. DOI: [10.1071/PH490214](https://doi.org/10.1071/PH490214).
- Wild J.P., McCready L.L. Observations of the spectrum of high-intensity solar radiation at metre wavelengths. *Austral. J. Sci. Res. A.* 1950, vol. 3, pp. 387–398. DOI: [10.1071/PH500387](https://doi.org/10.1071/PH500387).
- Wild J.P., Smerd S.F., Weiss A.A. Solar bursts. *Ann. Rev. Astron. Astrophys.* 1963, vol. 1, no. 1, pp. 291–366. DOI: [10.1146/annurev.aa.01.090163.001451](https://doi.org/10.1146/annurev.aa.01.090163.001451).
- URL: <http://ckp-rf.ru/usu/73606> (accessed September 16, 2021).
- URL: [https://www.atnf.csiro.au/pasa/17\\_1/cairns/paper/index.html](https://www.atnf.csiro.au/pasa/17_1/cairns/paper/index.html) (accessed September 17, 2021).
- URL: <https://hesperia.gsfc.nasa.gov/goes> (accessed September 16, 2021).
- URL: [https://www.noaa.gov/GOES/GOES\\_DCS/goes\\_dcs.html](https://www.noaa.gov/GOES/GOES_DCS/goes_dcs.html) (accessed September 16, 2021).
- URL: [https://www.sws.bom.gov.au/World\\_Data\\_Centre/1/9/6](https://www.sws.bom.gov.au/World_Data_Centre/1/9/6) (accessed September 16, 2021).
- URL: <https://sdo.gsfc.nasa.gov/data/aiahmi> (accessed September 16, 2021).
- URL: [https://www.sws.bom.gov.au/World\\_Data\\_Centre/1/9/5](https://www.sws.bom.gov.au/World_Data_Centre/1/9/5) (accessed September 17, 2021).
- URL: <https://www.slideserve.com/toussaint/srs-data-examples-powerpoint-ppt-presentation> (accessed September 16, 2021).
- URL: [https://suntoday.lmsal.com/suntoday/?suntoday\\_date=2019-05-06](https://suntoday.lmsal.com/suntoday/?suntoday_date=2019-05-06) (accessed September 17, 2021).
- URL: [https://aia.lmsal.com/aia\\_cadence/aia\\_0193\\_rdiff\\_0144\\_sum\\_20190506\\_0500/AIA\\_0193\\_RDIFF\\_0144\\_SUM\\_20190506\\_0500.html](https://aia.lmsal.com/aia_cadence/aia_0193_rdiff_0144_sum_20190506_0500/AIA_0193_RDIFF_0144_SUM_20190506_0500.html) (accessed September 17, 2021).
- Original Russian version: N.O. Muratova, A.Yu. Fedotova, J.N. Shamsutdinova, published in *Solnechno-zemnaya fizika*. 2022. Vol. 8. Iss. 1. P. 24–33. DOI: [10.12737/szf-81202203](https://doi.org/10.12737/szf-81202203). © 2022 INFRA-M Academic Publishing House (Nauchno-Izdatelskii Tsentr INFRA-M)

### How to cite this article

Muratova N.O., Fedotova A.Yu., Shamsutdinova J.N. Results of joint observations with solar spectropolarimeter of meter range wavelengths and other instruments. *Solar-Terrestrial Physics*. 2022. Vol. 8. Iss. 1. P. 24–33. DOI: [10.12737/stp-81202203](https://doi.org/10.12737/stp-81202203).